Imaging of One-Dimensional Conducting Pt Complexes Using Atomic Force Microscopy

Tatsuji Kawasaki,[†,††] Lei Jiang,[†] Tomokazu Iyoda,[†] Toshinari Araki,[††] Donald A. Tryk,[†††]
Kazuhito Hashimoto,[†,†††] and Akira Fujishima*[†,†††]
[†]*KAST Laboratory in Tokyo Institute of Polytechnics, 1583 Iiyama, Atsugi, Kanagawa 243-02*
[††]*Tokyo Gas Co., Ltd., 7-7, Suehiro-cho, 1-Chome, Tsurumi-ku, Yokohama 230*
[†††]*Department of Applied Chemistry, Faculty of Engineering, University of Tokyo, Hongo, Bunkyo-ku, Tokyo 113*

(Received June 29, 1995)

One-dimensional conducting Pt complexes were investigated by atomic force microscopy (AFM). In large scale images, layered structure was observed, which indicated a layer-spreading crystal growth mechanism. The molecular resolution images show the arrangement of the cyanide ligands on the (010) face with a=9.3 ± 0.4 Å and c=5.3 ± 0.4 Å.

One-dimensional (1D) conducting molecular systems are important for future applications involving electronic devices. The conductance of a 1D system, which is based on its geometric and electronic structure, is particularly influenced by its surface conductance. In order to improve the electrical properties of these materials, it is necessary to gain insight into the geometric and electronic structure of their surfaces. In order to better understand the nature of the surface, it is appealing to employ real-space techniques such as scanning tunneling microscopy (STM) and atomic force microscopy (AFM). Indeed, recent STM and AFM studies[1-5] have presented surface molecular images of several 1D-conducting systems, including both organic systems (e.g., conducting salts such as TTF-TCNQ and BEDT-TTF) and inorganic systems. These studies have provided much useful information on the surface structures and the crystal growth mechanisms. The most intensively studied inorganic 1D-conducting system has been the potassium tetracyanoplatinate bromide complex, KCP(Br).[6-9] High quality single crystals can easily be prepared via electrochemical synthesis[10] and the crystals have surfaces that are flat enough to be observed with AFM. The crystal structure has been established with X-ray and neutron diffraction.[11] However, the crystal growth mechanism and the dependence of the properties on the morphology and electronic states of the crystal are not fully understood, particularly at the molecular level.

The KCP(Br) crystals were prepared via the electrochemical synthetic method described previously.[12] The aqueous KBr solution (1.0 M, 2.4 mL) containing 300 mg of potassium tetracyanoplatinate(II) was placed in a 5 mL electrolysis cell. Two Pt wire electrodes were used with a controlled cell potential of 1.57 V. Needle-like crystals grew predominantly perpendicular to the surface of the Pt anode. Prior to the AFM measurements, the crystals were stored at 23 °C under a controlled relative humidity of 72% using a saturated solution of NH_4Cl and HNO_3.[13] Without any further treatment, the crystal was mounted on the AFM stage with the mirror-like side face of the needle crystal, (010) surface facing up. An SPA3000 AFM (Seiko Instruments) was used under ambient atmosphere conditions using Si_3N_4-coated cantilevers with an operating force of approximately 10 nN.

The KCP(Br) has a columnar structure consisting of staggered tetracyanoplatinate units.[14] The needle-like crystals (monoclinic space group P4mm) have unit cell dimensions as follows: a=b=9.906 Å and c=5.775 Å, as shown in the inset in Figure 3b.[15] The Pt-Pt distance along the column (2.89 Å) is close to that in Pt metal (2.78 Å), while the interchain Pt-Pt distance is larger (9.906 Å). This 1D-type structure results in anisotropic electrical conductivity, where the conductivity parallel to the Pt chains (c-axis) is much higher than that along the orthogonal a and b axes.

A high resolution AFM image obtained on one of the (010) terraces, covering 20 nm × 20 nm, is shown in Figure 1. Molecular rows can be observed. Figure 2 shows a magnified image (3.65 nm × 3.65 nm) in Figure 1. Here one can compare the structure with that determined crystallographically. Four neighboring bright spots exhibit a rectangular arrangement with edges of 9.3 ± 0.4 Å and 5.3 ± 0.4 Å, which corresponds to the arrangement of protruding cyanide ligands on the (010) surface. From this we can conclude that this magnified image corresponds to the molecular-level topography and reflects the columnar structure of the staggered tetracyanoplatinate units on

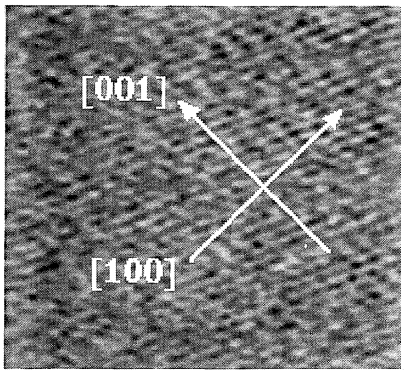

Figure 1. Small scale AFM image of the (010) face of KCP(Br) (20 nm × 20 nm, low-pass filtered image).

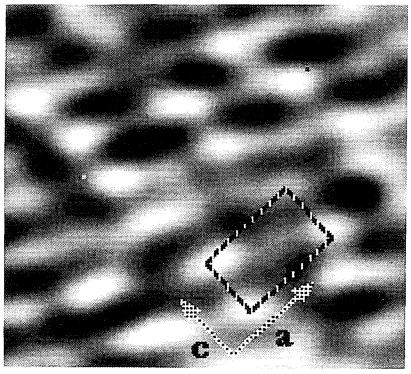

Figure 2. Molecular image of the (010) face (3.65 nm× 3.65 nm, magnified image in Figure 1).

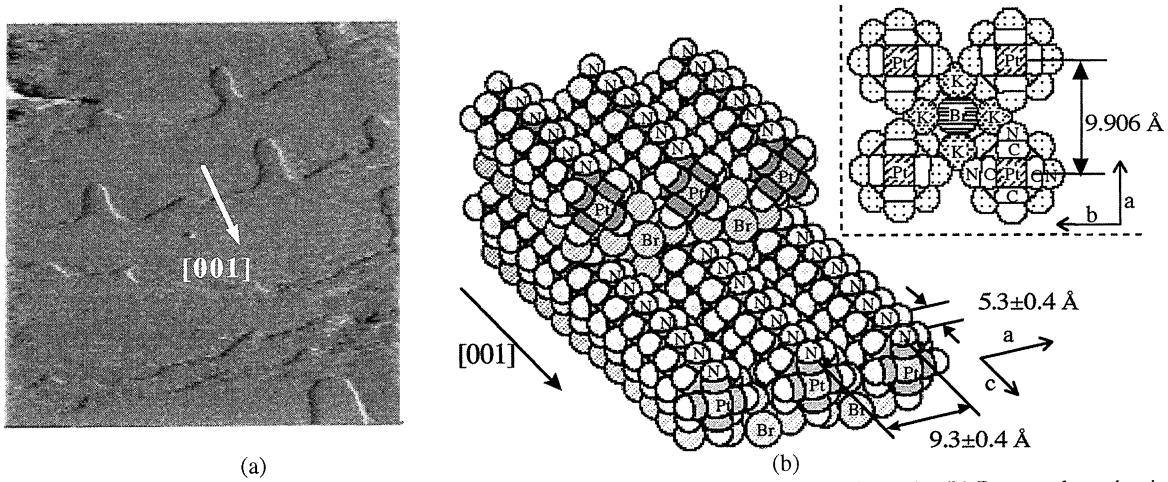

(a) (b)

Figure 3. (a) Large-scale AFM image of the (010) face of KCP(Br) (1.0 μm × 1.0 μm, raw AFM image). (b) Proposed mechanism of the layer-spreading crystal growth process.

the (010) face. The [001] and [100] directions are shown in Figure 1, considering molecular arrangement in Figure 2. The lattice parameters (a=b=9.3 ± 0.4 Å and c=5.3 ± 0.4 Å) observed here for the surface differ from those in the bulk (a=b=9.906 Å, c=5.775 Å) by a factor of approximately 0.93. The smaller lattice parameters may be due to a molecular arrangement specific to the surface. For example, KCP(Br) crystals tend to dehydrate. It has been reported in the literature that dehydration induces molecular rearrangements.[16] This would affect the surface more than the bulk. This may be a reasonable explanation since the crystal was exposed to the ambient, unhumidified atmosphere during the actual measurement. Further work is planned to be carried out under controlled humidity conditions.

We also examined the larger scale topography (1.0 μm × 1.0 μm) of the KCP(Br) crystals (Figure 3a). The observed (010) face exhibited very flat terraces with several steps. The step heights were about 1.0 nm, which is consistent with the unit cell parameters for the a and b axes (0.991 nm). Thus, the terraces appear to be monolayer. On the boundaries of the terraces, several rectangular hollows with [001] and [100] edges are arranged parallel to the c axis. We propose that this morphology results from a layer-spreading-type growth process, which occurs due to the anisotropic conductivity of the crystal. During crystal growth, it is supposed that $[Pt^{II}(CN)_4]^{2-}$ is oxidized to $[Pt^{IV}(CN)_4Br_2]^{2-}$ near the anode via redox mediation by electrogenerated Br_2, which was confirmed by voltammetric measurements.[17] In this case, the reactant and product crystallize on the anode in a ratio $K_2[Pt(CN)_4]$:$K_2[Pt(CN)_4Br_2]$ of 5:1. The AFM images (Figure 3a) show atomically flat terraces with no domains. Since no nuclei were observed on the terraces, we propose that the layer edges play a role as growth sites for crystallization. These edges essentially act as line-type microelectrodes for the growth of the layer. The electrons can move along the high-conductivity c axis from the edge of the layer next to the Pt anode so that $K_2[Pt(CN)_4]$ can then be oxidized at the edge of the layer away from the Pt anode.

There are actually two growth modes. After very thin whisker-like crystals are formed in the primary stage on the electrode, one mode involves growth along the c axis from the edges of the monolayers, as just described. The other involves growth along the a and b axes starting from the electrode surface between the whiskers. Our in situ optical microscopic observation of the crystal growth also showed that the growth rate along the c axis is much faster than that along the a and b axes. Thus, the whisker-like crystals grow continuously in a layer-spreading process. The second growth mechanism accounts for the thickening of the whiskers to form needle-like crystals.

In summary, the large-scale AFM images show layered structures indicating a layer-spreading crystal growth mechanism. The monolayer thickness agrees well with the thickness of the tetracyanoplatinate column along the a and b axes. The molecular resolution image of the surface topography on the (010) face corresponds to the arrangement of the cyanide ligands, with lattice parameters a=b=9.3 ± 0.4 Å and c=5.3 ± 0.4 Å, where the observed spots correspond to nitrogen atoms of the cyanide ligands that protrude from the surface.

References

1 C. H. Hillier and D. W. Michael, *Science*, **265**, 1261 (1994).
2 S. N. Magonov and M.H.Whangbo, *Adv. Mater.*, **6**, 355 (1994).
3 J. H. Schott, C. M. Yip and M. D. Ward, *Langmuir*, **11**, 177 (1995).
4 S. N. Magonov, G. Bar, A. Y. Gorenberg, E. B. Yagubskii and H. J. Cantow, *Adv. Mater.* , **5**, 453 (1993).
5 G. B. Scott, S. R. Johnson, B. I. Swanson, J. Ren and M. H. Whangbo, *Chem. Mater.*, **7**, 391 (1995).
6 J. S. Miller, A. J. Epstein, *Prog. Inorg. Chem.*, **20**, 1(1976).
7 H. J. Keller, in "Extended Linear Chain Compounds, " ed by J. S. Miller, Plenum, New York (1982) vol. 1.
8 I. F. Shchegolev, *Phys. Stat. Sol.(a)*, **12**, 9 (1972).
9 M. J. Rice, *Phys. Bull.*, **26**, 493 (1975).
10 J. S. Miller, *Science*, **193**, 189 (1976).
11 H. J. Deiseroth and H. Schulz, *Phys. Rev. Lett.*, **33**, 963 (1974).
12 J. S. Miller, in "Inorganic Synthesis," ed by D. F. Shriver, John Wiley and Sons, New York (1979) vol. 19, 13.
13 D. Kuse and H. R. Zeller, *Solid State Commun.*, **11**, 355 (1972).
14 K. Krogmann, *Angew. Chem. , Internat. Edit.*, **8**, 35 (1969).
15 J. M. Williams, J. L. Petersen, H. M. Gerdes and S. W. Peterson, *Phys. Rev. Lett.*, **33**, 1079 (1974).
16 D. Cahen, *Solid State Commun.*, **12**, 109 (1973).
17 T. Kawasaki, L. Jiang, T. Iyoda, K. Hashimoto and A. Fujishima, unpublished results.